ADVANCED FUNCTIONAL MATERIALS
www.afm-journal.de

Bioinspired Ultra-Stretchable and Highly Sensitive Structural Color Electronic Skins

Yuanyuan Shang, Chao Huang, Zhou Li, and Xuemin Du**

Organisms possess remarkably adaptive ability to complex environments. For example, chameleons can alter their skin color to adapt to varying environments, which has inspired significant advances in bioinspired soft electronic skins (E-skins), and their wide applications in wearable sensors, intelligent robots, and health monitoring. However, current bioinspired E-skins face challenges in ultra-stretchability, high sensitivity, and long-term stability owing to the intrinsic limitations associated with their mismatched interface between soft matrix and hard conductive fillers, hindering their practical applications. Here, it is reported that bioinspired structural color electronic skins (SC E-skins) that consist of liquid metal particles (LMPs), periodical ordered colloidal crystal arrays, and ultra-stretchable hydrogel, imparting synergistic and durable electrical–optical sensing capabilities. Such SC E-skins demonstrate outstanding performances including superior flexibility (elongation at break > 1100%), high sensitivity (gauge factor = 3.26), fast synergetic electric–optical response time (≈100 ms), outstanding durability (over 1500 cycles), and high accuracy (R^2 > 99.5%). These bioinspired SC E-skins with excellent capability of converting mechanical signals into synergetic electrical–optical outputs hold great promise for smart wearable devices, affording a new horizon in developing advanced health monitoring technologies.

1. Introduction

In nature, organisms such as chameleons and octopuses possess the remarkable ability to sense external stimuli rapidly and adapt their behaviors to complex environments (**Figure 1A**).[1–5] These behaviors are generally mediated by neuromuscular organs that involve a combination of neural electrical impulses and muscle relaxation/contraction, allowing them to dynamically alter their appearances in responding to diverse environmental stimuli. Inspired by these biological features, various electronic skins (E-skins) have been developed, showing great potential in the emerging fields of soft robots,[6] Internet of Things,[7] neural interfaces,[8] and healthcare monitoring.[9,10] Graphene,[11] carbon nanotubes, metal nanowires,[12] or conductive polymers[13] embedded or integrated with stretchable elastomers,[14,15] hydrogels,[16] or transistors[17] endow E-skins electrical sensing capability. Among them, hydrogel-based E-skins are attractive due to the intriguing advantages of hydrogels including good biocompatibility, excellent flexibility, and tissue-like mechanical properties.[18–27] These hydrogel-based E-skins can accurately sense and convert external mechanical stimuli into electric signal outputs. However, these electronic skins can solely display a single mode of electric signals, which still lack visual feedback capability similar to chameleons, thus hindering their practical applications, especially in human–machine interactions.[28–30]

To address the above-mentioned challenges, great efforts have been devoted to integrating various color elements such as phosphors,[31] fluorescent molecules,[32] dyes, and pigments,[33] into hydrogel-based E-skins, realizing electrical–optical dual sensing. However, these colorimetric E-skins suffer from low-contrast, slow-response, and easy photobleaching issues owing to the inherent disadvantages of these color elements.[34,35] In contrast, chameleon-inspired structural color materials constructed with periodic micro-/nano-structures offer unique advantages such as high contrast, fast response, and superior stability.[36–50] By incorporating structural color elements and hard conductive fillers, hydrogel-based E-skins can achieve rapid electrical sensing and brilliant optical visualization simultaneously in response to pressure or strain.[51–55] Despite significant progress, current

Y. Shang, Z. Li
School of Chemistry and Chemical Engineering
Center on Nanoenergy Research
Guangxi University
Nanning 530004, China
E-mail: zli@binn.cas.cn
Y. Shang, C. Huang, X. Du
Center for Intelligent Biomedical Materials and Devices (IBMD)
Shenzhen Institute of Advanced Technology (SIAT)
Chinese Academy of Sciences (CAS)
Shenzhen 518055, China
E-mail: xm.du@siat.ac.cn
Y. Shang, Z. Li
Beijing Institute of Nanoenergy and Nanosystems
Chinese Academy of Sciences
Beijing 101400, China
X. Du
Key Laboratory of Biomedical Imaging Science and System
Chinese Academy of Sciences
Shenzhen 518055, China

The ORCID identification number(s) for the author(s) of this article can be found under https://doi.org/10.1002/adfm.202412703

DOI: 10.1002/adfm.202412703

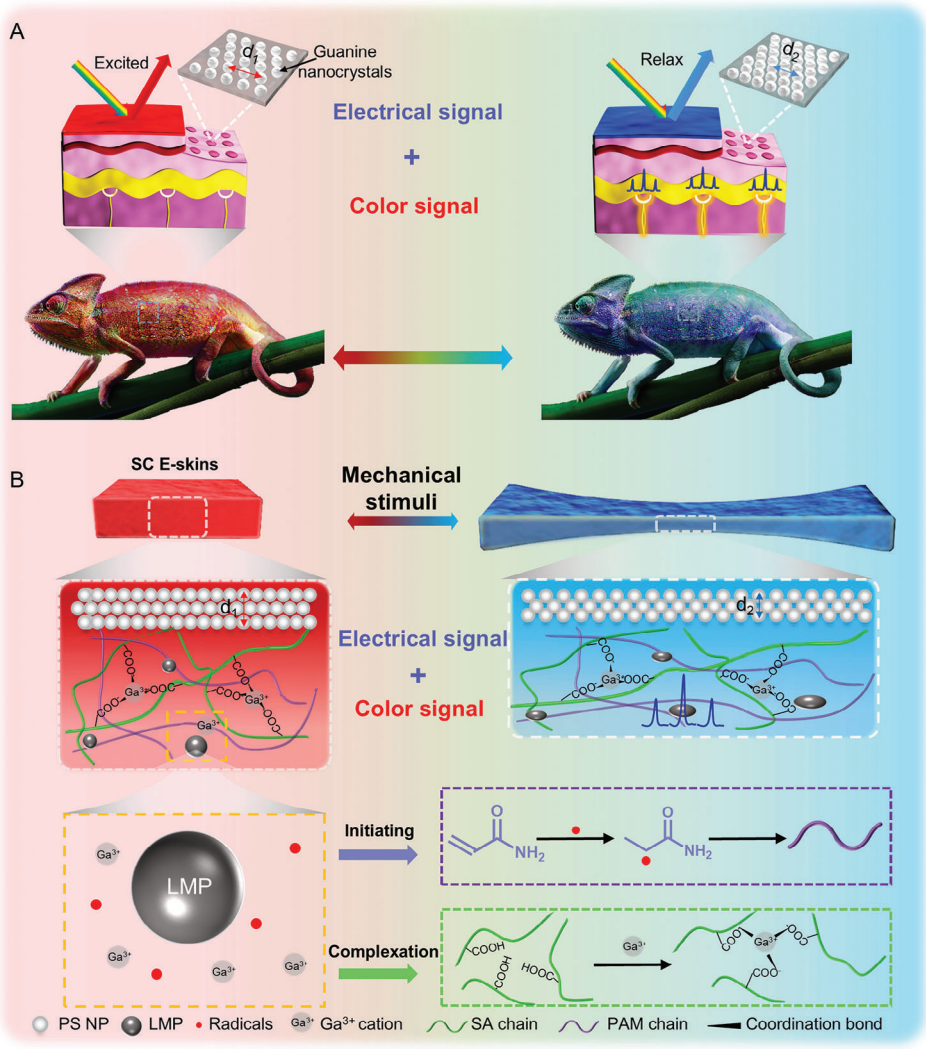

Figure 1. Bioinspired design of the SC E-skins. A) Schematically illustrating the chameleon's skin to sense the environmental stimuli and transmit the stimuli into nerve electrical signals and color signals. B) Schematically illustrating the SC E-skins to sense mechanical stimuli and transmit the stimuli into electrical and color signals. The LMPs embedded in the SC-E skins act the multifunctional roles, generating radicals to initiate the polymerization of acrylamide and releasing Ga^{3+} to complex with sodium alginate, finally resulting in the PAM/SA-GA^{3+} double-network hydrogel.

structural color E-skins still face challenges in achieving superior performance, especially in terms of ultra-stretchability, high sensitivity, and long-term stability in electrical and/or optical signal output, which is attributed to the intrinsic limitations associated with the interfacial mismatch between soft matrix and hard conductive fillers.[56] Therefore, it is highly crucial to develop structural color E-skins with satisfactory performances for human–machine interaction.[14,30,53,55,57]

In this work, we report bioinspired structural color electronic skins (SC E-skins) that integrate periodically ordered colloidal crystal arrays with double-network hydrogel (i.e., liquid metal particles (LMPs) embedded within polyacrylamide/sodium alginate, PAM/SA-Ga^{3+}), imparting synergetic electric–optical sensing and superior mechanical properties. Benefiting from the unique activities, the LMPs not only initiate free radical polymerization to form PAM hydrogel networks but also serve as the physical cross-linkers for forming SA-Ga^{3+} hydrogel networks (Figure 1B).[58–60] Harnessing the robust interaction of LMPs with the double-network hydrogel as well as their unique fluidity and high conductivity, our SC E-skins with unique interface between the hydrogel matrix and fluidic conductive fillers demonstrate outstanding performances including superior flexibility (elongation at break > 1000%), high sensitivity (gauge factor = 3.26), fast synergetic electric–optical response time (≈100 ms), outstanding durability (over 1500 cycles), and high accuracy (R^2 > 99.5%). These bioinspired SC E-skins with the excellent capability of converting one mechanical signal into two outputs hold great promise for practical applications, especially in human–machine interaction scenarios.

2. Results and Discussion

2.1. Fabrication of SC E-Skins

The SC E-skin consists of a structural color layer and a conductive double-network hydrogel layer (**Figure 2**A). To fabricate the SC E-skin, we first assembled monodispersed polystyrene (PS) nanoparticles into ordered colloidal crystal arrays to form the structural color layer (Figure S1, Supporting Information).[61] Next, a conductive hydrogel precursor was prepared by adding well-dispersed gallium–indium alloyed liquid metal particles (LMPs) (Figure S2, Supporting Information) into the mixture of acrylamide (AM), sodium alginate (SA), initiator ammonium persulfate (APS), and the cross-linker *N, N'*-methylene-bisacrylamide (NMBA), and then poured into the structural color layer. Finally, the SC E-skin was obtained by curing the conductive double-network hydrogel in the voids of the colloidal crystal arrays at room temperature.

Notably, the LMPs can also promote the formation of the double-network hydrogel by both initiating the polymerization of AM through generating radicals and releasing Ga^{3+} to coordinate with SA (Figure 2A).[58–60,62] Electron paramagnetic resonance (EPR) confirmed the generation of sulfate radicals in the above precursor due to the presence of LMPs, and the incubation of the precursor and the DMPO could result in the visible EPR spectra at 1 min as shown in Figure 2B. As evident, the existence of LMPs significantly activated the APS molecule via generating $SO_4^{-}\cdot$ and the characteristic sulfate radical signal (2:2:1:2:1:2) could be observed in the precursor of the SC E-skin,[63] which is otherwise impossible in the LMPs-free samples. These unique activities of the LMPs enable radical polymerization of the AM monomers into the PAM chains at room temperature, whereas the polymerization could not occur in the absence of LMPs. Additionally, inductively coupled plasma optical emission spectra (ICP-OES) further showed that the LMPs could also release Ga^{3+} (Figure S3, Supporting Information), which could form coordination bonds with the SA as validated by the Fourier transform infrared spectroscopy (FTIR) absorption at 1612 cm^{-1} (Figure 2C), corresponding to the characteristic peak of coordination bonds between Ga^{3+} and —COO^{-} of SA.[64] SEM images showed that the LMPs were homogeneously dispersed in the conductive hydrogel layer of the SC E-skins (Figure 2D,F), and the superior electrical conductivity of the LMPs endows the SC E-skins with excellent conductivity, which increases from 0.073 to 0.140 $S\cdot m^{-1}$ with an increase of the LMPs content from 4 wt.% to 18 wt.% as shown in Figure 2G. Interestingly, the dark color of the LMPs increases the color contrast of the SC E-skin, which displays a vivid red color from the periodically arranged 200-nm colloidal nanoparticles (Figure 2H; Figure S4, Supporting Information). With an increase of the LMPs content from 4 wt.% to 18 wt.%, the reflectance of the SC E-skins red-shifts from 599 to 657 nm, and the relative intensity increases from 50% to 80% (Figure 2I). In addition, the stretchability of SC E-skins also increases from 1160% to 1290% with an increase of the LMPs contents from 4 wt.% to 18 wt.% (Figure 2J), ascribing to the formation of double-network PAM/SA-Ga^{3+} hydrogel (Figure S5, Supporting Information). Overall, we found that the SC E-skins with 18 wt.% LMPs showed the highest conductivity and the brightest structural color, while further increasing the LMPs content to 21 wt.% led to too fast polymerization of the conductive layer and thereby difficult infiltration of the precursor into the structural color layer (Figure S6, Supporting Information).

2.2. Electrical Sensing Performances

We first evaluated the electrical sensing performances of SC E-skins to strain. We found that the resistance of the SC E-skins increased with the increase of strain (from 40.7 to 123.9 kΩ corresponding to the strain from 0% to 100%; **Figure 3**A; Figure S7, Supporting Information). Owing to the excellent fluidity of the LMPs and hydrogen bonding between the LMPs and polymer chains in the hydrogels,[65] they can be deformed with the stretching of the hydrogel matrix (Figure S8, Supporting Information). Therefore, there are no interfacial voids between the LMPs and hydrogel even under stretch, which provides the possibility of sensing a large range of strain. We next quantitively evaluated the strain with respect to the relative resistance change ($\Delta R/R_0$), which was calculated according to the following equation:

$$\Delta R/R_0 = \left(R - R_0\right)/R_0 \tag{1}$$

where R_0 is the original resistance and R refers to the real-time characterized resistance. Due to ultra-stretchability, the SC E-skins can not only precisely detect the strain that human skin can tolerate (from 0% to 4.8% corresponding to the strain from 0–30%) (Figure 3B–D),[66] but also monitor the extensive strain (from 4.8% to 531% corresponding to the strain from 30–200%) beyond the human skin (Figure 3E), indicating the implications of the SC E-skins to soft robotics especially in the scenarios involving ultrahigh stretch. In addition, we also calculated the gauge factor (GF) of the SC E-skins for assessing the sensitivity of the electrical signals to strain. When the SC E-skins are stretched at the range of 0%–30%, 30%–100%, and 100%–200%, the GF value is calculated to be 1.63, 2.31, and 3.26, respectively (Figure 3F). Besides the broad detection range and high sensitivity, the SC E-skins can instantly respond to 100% strain with a high frequency of 0.5 Hz owing to the excellent fluidity of LMPs (Figure 3G). In addition, because of the seamless and stable interface between the LMPs and hydrogel matrix, the SC E-skins exhibit consistent electrical conductivity over 1500 cycles of 50% strain (Figure 3H), indicating that the SC E-skins possess superior durability for long-term usage.

2.3. Optical Sensing Performance

As compared to conventional E-skins with single feedback, our SC E-skins provide an extra route to sense strain by optical signals that can be facilely recognized by the naked eye (**Figure 4**A). To investigate the optical sensing performance, we characterized the color changes of the SC E-skins under different strains (from 0% to 70%), observing that the structural color of the SC E-skins sequentially changed from red to green and ultimately to blue, and the reflection peak of the SC E-skin gradually shifted from 628 to 505 nm (Figure 4B).

To further investigate the mechanism of color change in response to strain, we characterized the lattice distance of colloidal

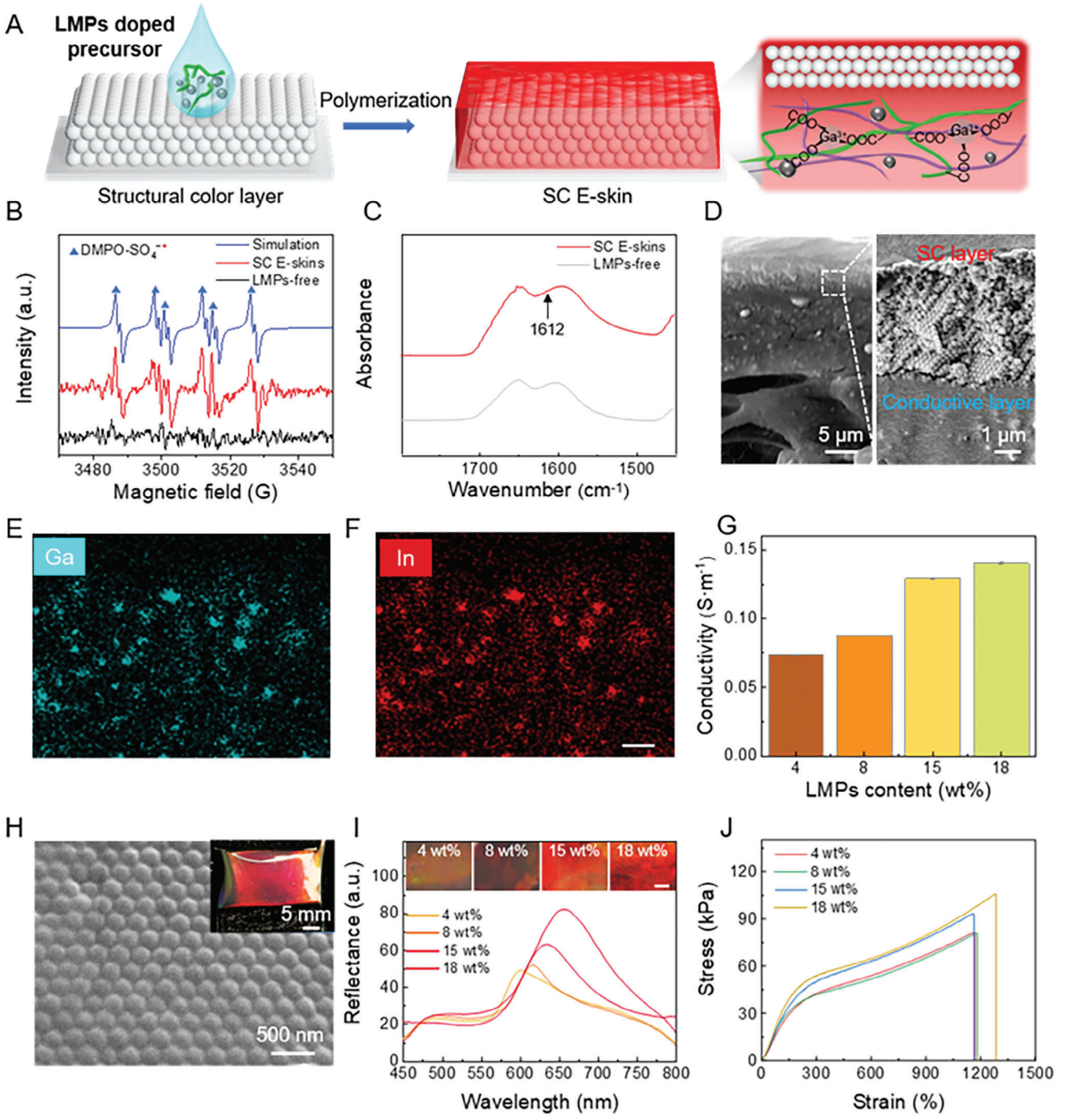

Figure 2. Preparation of the SC E-skins. A) Schematic diagram of the preparation of the SC E-skins and the formation of the PAM/SA-Ga^{3+} hydrogel involving sulfate radicals and Ga^{3+} cross-linkers generated from LMPs. B) Electron paramagnetic resonance (EPR) spectra of 5, 5-dimethyl-1-pyrroline *N*-oxide (DMPO)-SO_4^{-}· (blue), SC E-skins (red), and LMPs-free samples (black), respectively. C) FTIR spectra of SC E-skins and LMPs-free samples. D) Representative cross-section scanning electron microscopic (SEM) images of the SC E-skins. The inset is a high-magnification SEM image that shows a seamless interface between the structural color layer and the conductive hydrogel layer. E, F) Energy dispersive spectral (EDS) mapping of the cross-section of the SC E-skins. Scale bar: 5 μm. G) The conductivity of the SC E-skins with different LMPs contents (4, 8, 15, and18 wt.%). H) SEM and macroscopic pictures (inset) of the structural color layer. Scale bars: 500 nm and 5 mm (inset). I) The macroscopic photos and reflection spectra of the SC E-skins with different LMPs contents. Scale bar: 500 μm. J) Stress–strain curves of the SC E-skins with different LMPs contents.

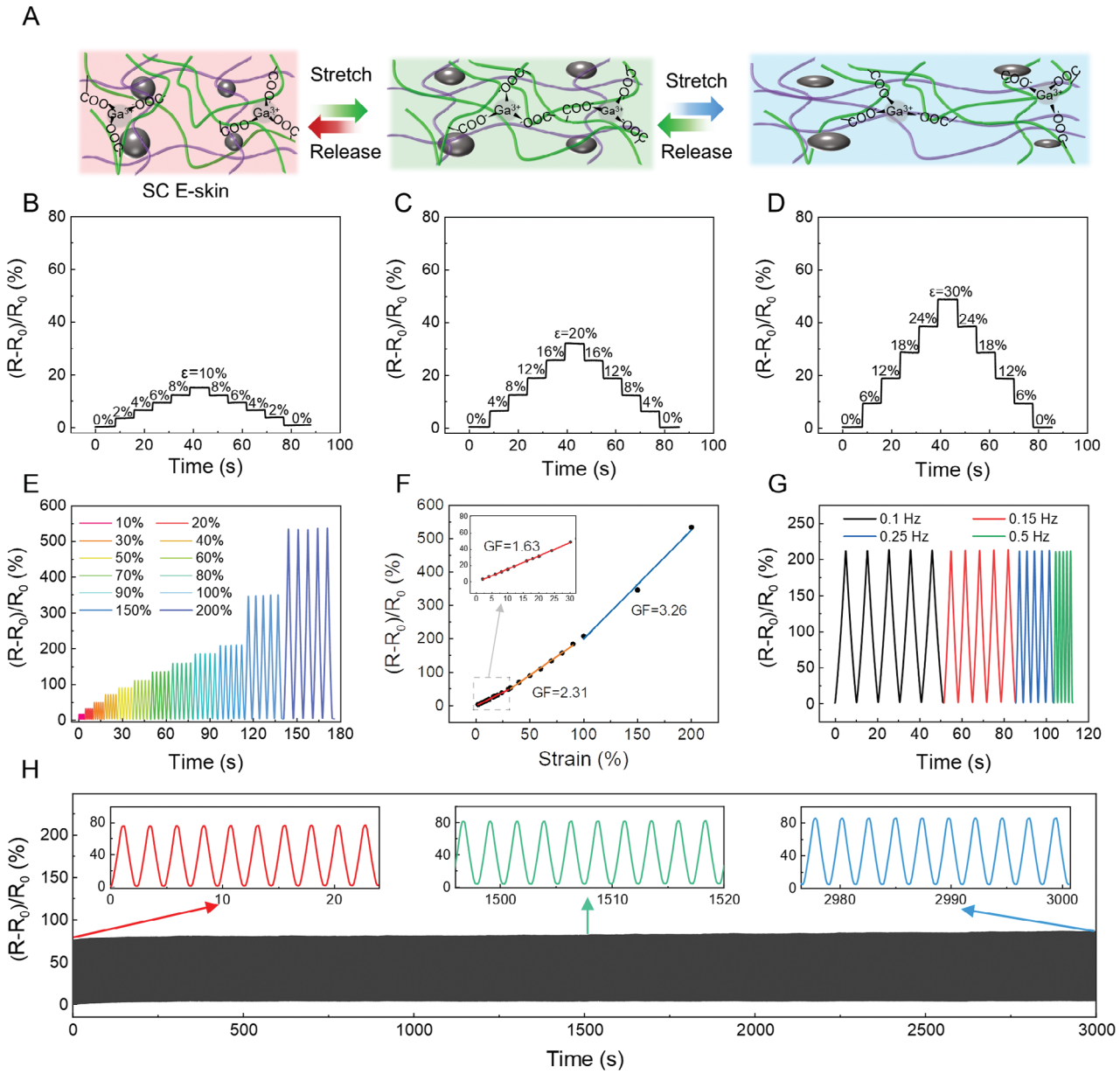

Figure 3. Electrical sensing performances of the SC E-skins. A) Schematic diagram of the SC E-skin to sense strain via electrical signals. B–D) Relative resistance change of the SC E-skins under the strain of 10% (B), 20% (C), and 30% (D). E) Relative resistance changes under different strains from 10% to 200%. F) The relative resistance–strain curve with calculated gauge factors (GFs) of the SC E-skins. G) Relative resistance changes of the SC E-skin in response to 100% strain with frequency of 0.1, 0.15, 0.25, or 0.5 Hz. (H) Relative resistance changes of the SC E-skins under 1500 cycles of 50% strain.

nanoparticles during the stretch. The cross-sectional SEM images of the SC E-skins under strain show the lattice distance of the colloidal nanoparticles reduced from 192 to 154 nm corresponding to the strain from 0% to 70% (Figure S9, Supporting Information). According to the Bragg-Snell equation as follows:

$$\lambda_{max} = 1.633 \frac{d}{m} \sqrt{\sum n_i^2 V_i - \sin^2\theta} \quad (2)$$

where λ_{max} is the reflection peak of the structural color; d is the diameter of the PS nanoparticles; m is the order of Bragg diffraction; n_i and V_i are the refractive index and volume fraction of the PS nanoparticles or hydrogel matrix; and θ is the incident angle of the light. The decrease in the lattice distance of the colloidal nanoparticles (d) would lead to the decrease in λ_{max} and thereby the blueshift of the SC E-skin under strain.

We then evaluated the optical sensing performance of the SC-E skin to strain including detection range, sensitivity, durability, and response time. Due to the stretchability of the double-network hydrogel layer, the SC E-skins could monitor the large strain up to 200%, as indicated by the changed color from red to purple (Figure S10, Supporting Information). Besides facilely

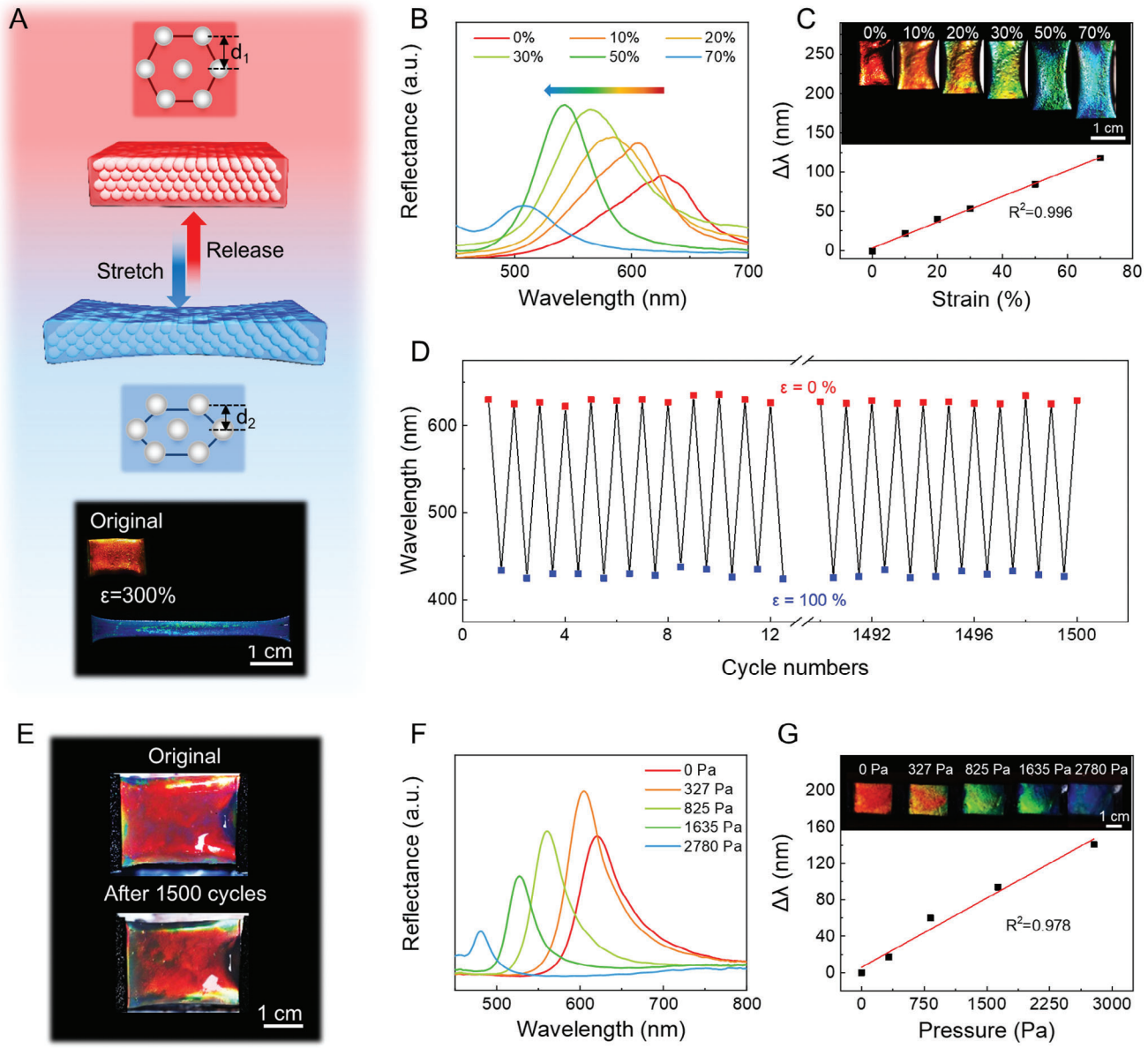

Figure 4. Optical sensing performance of the SC E-skins. A) Schematic diagram and macroscopic photos of the SC E-skins under stretch. B) The reflection spectra of the SC E-skins under strain. C) Optical images and the change of reflection of the SC E-skin under different strains (0 to 70%). Scale bar: 1 cm. D) The reflection peak values of the SC E-skin under 1500 stretch-relaxation cycles. E) Macroscopic images of the SC E-skins before and after the 1500 stretch-relaxation cycles. Scale bar: 1 cm. F) The reflection spectra of the SC E-skins under different pressures (0, 327, 825, 1635, or 2780 Pa). G) Macroscopic images and the change of reflection of the SC E-skins under different pressures. Scale bar: 1 cm.

colorimetric monitoring, the SC E-skin could also precisely detect the strain with the assistance of a fiber-optic spectrometer. The reflection peak shift of the SC E-skins was perfectly linearly with strain (R^2 = 0.995) following the Bragg-Snell equation (Figure 4C), offering a quantitative way for precisely monitoring strain. The mechano-chromic sensitivity of the SC E-skin is as high as 1.64 nm per 1% strain. Besides, the SC E-skins possess stable and reliable optical signal outputs during repeated deformations (over 1500 times; Figure 4D). The original colors of the SC E-skins could also be well preserved after 1500 cycles (Figure 4E). Furthermore, the SC E-skins also possess fast (≈100 ms) and accurate (R^2 = 0.999 and 0.996 for electrical and optical sensing, respectively) synergetic electrical–optical response to strain (Figure S11, Supporting Information), implying attractive potential in visualized health monitoring. Remarkably, under a low temperature (0 °C) and near body temperature (40 °C), the SC E-skins are still ultra-stretchable and can reliably sense 100% strain with a fast response time of 100 ms via synergistic electrical and optical signals, behaving similarly to that at room temperature (Figures S12 and S13, Supporting Information), which is arisen by stable electrical properties of Ga-In LMPs within a wide temperature range (-60–60 °C).[67] These results

indicate the versatile potential of the SC E-skins under complex environmental conditions.

In addition to sensing strain, the SC E-skin could also monitor the pressure via the structural color change due to the reduction of lattice distance along the vertical direction under pressure. Even undergoing a slight pressure (2380 Pa), the SC E-skins can exhibit an obvious blueshift in color (from red to blue, corresponding to the reflection from 620 to 480 nm; Figure 4F,G), where the change of reflection ($\Delta\lambda$) shows a linear correlation with respect to the pressure ($R^2 = 0.978$). The sensitivity of the SC E-skin in sensing pressure is as high as 5.9×10^{-2} nm·Pa^{-1}, implying the promise of the SC E-skins in sensing slight pressure such as breath monitoring. Meanwhile, the SC E-skins could also precisely monitor the pressure via relative resistance, revealing their synergetic electrical and optical sensing capabilities to pressure (Figure S14, Supporting Information). Considering their outstanding sensing performances to multimodal mechanical stimuli (both strain and pressure), the SC E-skins would be greatly promising for human–machine interactions.

2.4. Applications of the SC E-Skins

Notably, the SC E-skins further demonstrate versatile adhesion to diverse surfaces such as rubber and biological skins, attaining the interfacial strength of 23.52 and 14.83 kPa, respectively (Figure S15, Supporting Information). Such versatile adhesion of the SC E-skins is attributed to the mechanical interlock caused by the roughness of substrate surfaces (e.g., balloon), dense packed noncovalent interaction formed between the hydrogel and substrate surfaces, and strong energy dissipation that contains the separation of intertwined PAM/SA chains.[58,68] Leveraging on the outstanding synergetic electrical–optical sensing performances and versatile adhesion, the SC E-skins impart various attractive potential applications. As shown in **Figure 5**A, an SC E-skin is adhered to a balloon. When the curvature of the balloon changes from 43 to 32 m^{-1} (≈26%), the color of the SC E-skin changes from red to blue ($\Delta\lambda = 127$ nm) as shown in Figure 5B. Correspondingly, the resistance of the SC E-skin increases from 1.64 to 4.38 kΩ (Figure 5C). Such SC E-skins showing synergetic electrical–optical response to curvature hold attractive promise for monitoring curvature changes of biological tissues by the naked eye such as alteration of intraocular pressure or growth of plants.[48,69]

In addition, the SC E-skins are also capable of monitoring the dynamic bending of our fingers (Figure 5D). The SC E-skins on the joint can change their structural color from red to blue (Bragg diffraction blue shifts from 632 to 473 nm) as the bending angle of fingers increases from 0° to 75° (Figure 5E), providing a promising prospect for visualized monitoring of the gesture. Moreover, The SC E-skins show synergetic electric–optical response to the bending angles of fingers, where the change of reflection and the relative resistance change both exhibit real-time response to bending angles (Figure 5F), offering the possibility of precise gesture recognition.

Breath monitoring is critical for diagnosing chronic respiratory diseases, whereas current approaches require complicated facilities and professional operators.[70] The SC E-skin shows the promise of addressing these challenges by facilely monitoring breath via the naked eye. After adhering to the rat's skin (Figure 5G), the SC E-skin could reliably monitor the breath of the rat due to their high sensitivity to slight strain. During the breath–relaxation cycles, the structural color of the SC E-skin changes between red and orange reversibly (Figure 5H), providing a convenient visible method for breath monitoring. Moreover, the breath rate of the rat could also be reflected by the relative resistance change and the change of reflection of the SC E-skins (Figure 5I), offering the possibility of precise breath monitoring. Remarkably, the SC E-skins exhibit good stability in the breath monitoring scenario (Figure 5I). For other specific practical applications, these hydrogel-based electronics can be further packaged or combined with superior hydrophilic polymers, organic solvents, and salts to avoid water evaporation.[71–74] The SC E-skins demonstrate exceptional mechanical properties and distinctive electric–optical dual outputs, holding great promise for health monitoring.

3. Conclusion

In summary, we developed the SC E-skins with a synergetic electrical–optical response by integrating LMPs-based hydrogel with periodically ordered colloidal crystal arrays. Within the SC E-skin, the fluidic LMPs not only act as the conductive fillers but also assist the formation of the PAM/SA-Ga^{3+} double-network hydrogel, imparting the SC E-skins with outstanding performances (Table S1) including superior flexibility (elongation at break > 1100%), high sensitivity (gauge factor = 3.26), fast synergetic electric–optical response time (≈100 ms), outstanding durability (over 1500 cycles), and high accuracy ($R^2 > 99.5\%$). The SC E-skins enable synergetic electrical–optical feedback by converting one mechanical signal into two outputs, realizing visible and accurate monitoring of curvature, finger bending, and breath, which holds great promise for intelligent health monitoring and human–machine interaction fields.[75–77]

4. Experimental Section

Materials: Styrene (St, 99%), acrylic acid (AA, 99%), potassium persulfate (KPS, 99%), acrylamide (AM, 99%), sodium alginate (SA), ammonium persulfate (APS, 99%), *N, N*-methylene-bis-acrylamide (NMBA, 99%) methylcellulose (MC) and sodium hydroxide (NaOH, 99.0%) were purchased from Sigma–Aldrich (Missouri, US). 5, 5-dimethyl-1-pyrroline *N*-oxide (DMPO, 99.0%) was purchased from Aladdin (Shanghai, China). Liquid metal (LM, eutectic gallium (Ga, 75.5%)-indium (In, 24.5%)) was obtained from Fanyada Electronic Technology Co., Ltd. (Zhenjiang, China). All chemicals except styrene were used as received without further purification. Styrene was purified by treating with a 5.0 wt.% aqueous NaOH solution to remove the inhibitor. Ultrapure water (18.2 MΩ·cm) was produced from a water purification system (Arioso Power II, Human, Korea) was used throughout this study.

Preparation of Monodispersed PS Particles and Structural Color Layer: Monodispersed PS particles were synthesized by emulsifier-free emulsion polymerization in a three-necked round bottom flask with a reflux condenser.[61,75] In a typical experiment, monodispersed PS particles (d: ≈ 200 nm) were prepared by adding 35 g St, 2 g AA, and 200 mL ultrapure water into a 500 mL flask. After the mixture was refluxed at 110 °C for 15 min, 10 mL 3.5 w/v% aqueous KPS solution was added under steady stirring at 300 rpm, followed by continued reflux at 110 °C for 3 h. The as-synthesized colloidal particles were collected by centrifugation at 16 500 rpm for 20 min three times, and the concentration of PS was adjusted to 4.0 wt.%. Glass

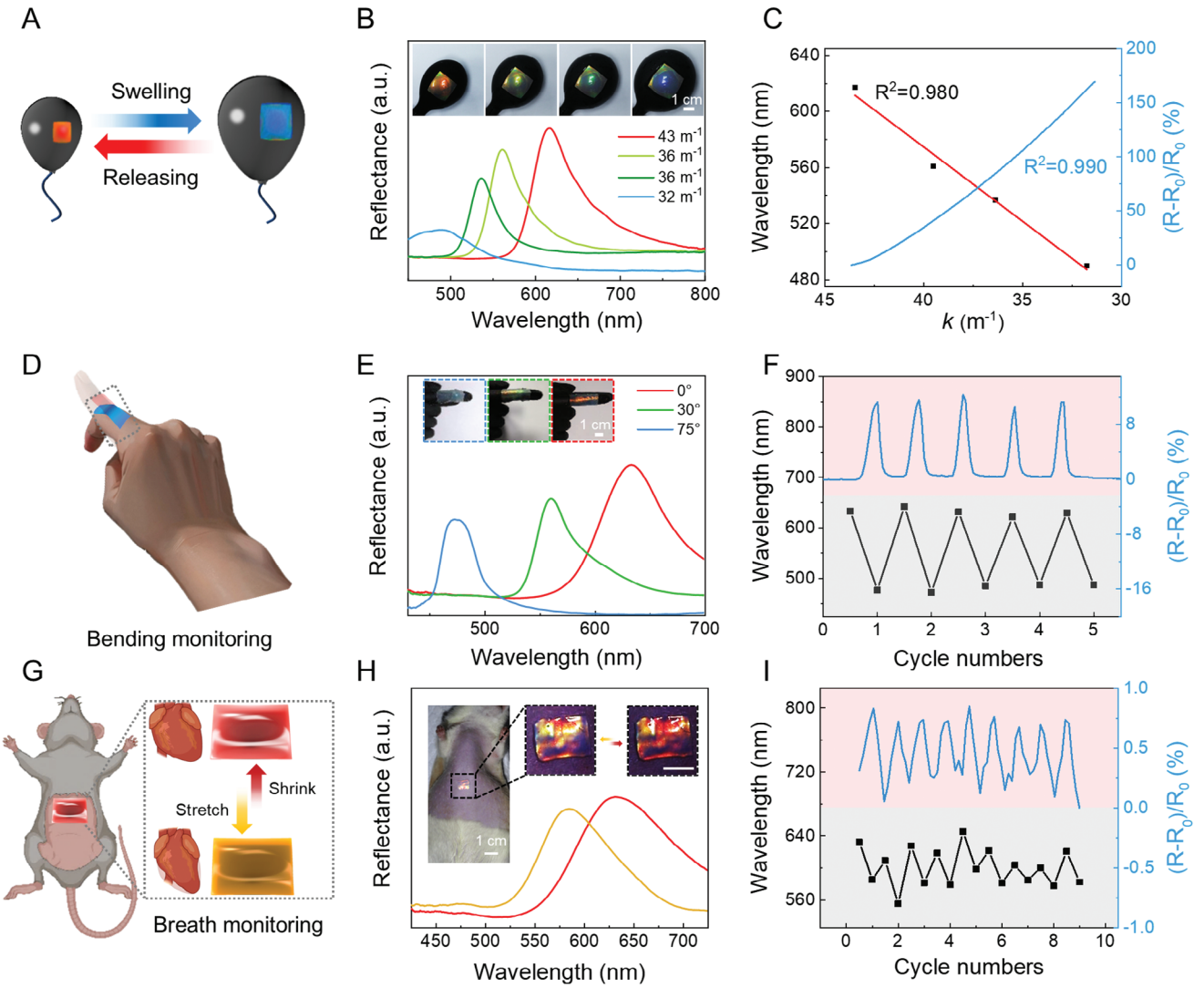

Figure 5. Applications of the SC E-skins. A) The schematic diagram of the SC E-skins on an expanding balloon. B) Macroscopic photos and reflection spectra of the SC E-skins on the expanding balloon under different curvatures. C) The synergetic electrical–optical sensing performance of the SC E-skins to the curvature of the balloon. D) The schematic diagram of the SC E-skins on the bending fingers. (E) Macroscopic photos and reflection spectra of the SC E-skins patched on a bending finger with different angles. Scale bar is 1 cm. F) The synergetic electrical–optical sensing performance of the SC E-skins to reversible finger bending between 0° and 75°. G) The schematic diagram of the SC E-skins on the rat's skin. H) Macroscopic photos and reflection spectra of the SC E-skins adhered to the rat's skin for breath monitoring. Scale bar: 1 cm. I) The synergetic electrical–optical sensing performance of the SC E-skins adhered to the rat's skin during its breath.

slides were cleaned by ultrasonic treatment in deionized water, ethanol, and oxygen plasma treatment for 3 min (PDC-MG, Mingheng, China). The structural color layer was obtained by dropping 80 µL PS latex on a treated glass slide (length × width = 25 mm × 25 mm) and assembled at room temperature for 12 h.

Preparation of LMPs: According to previous work, 0.05 g methyl cellulose was dissolved in 50 mL ultrapure water at 80 °C. After cooling down to room temperature (22 °C), 1.0, 2.0, 3.0, 4.0, 5.0, and 6.0 g LM were added into the prepared methylcellulose aqueous solution, respectively. Afterward, the mixtures were sonicated (KQ5200DE, Shumei, China) at a power density of 200 W in an ice bath for 2 h to obtain a LMPs suspension with the concentrations of 2, 4, 6, 8, 10, and 12 w/v%.[76–79]

Preparation of PAM/SA Hydrogel: The hydrogels with different AM-to-SA ratios and cross-linking agent concentrations were prepared. First, the mass ratios between AM and SA were changed. In a typical experiment, 10.0 g AM, 0.10 g APS, 0.01 g NMBA, and 50 mL ultrapure water were added to a glass bottle. SA with different weights of 1.0, 2.0, or 3.0 g were added into the above solutions and stirred until being completely dissolved. The hydrogel was then cured by heating at 50 °C for 2 h. Second, the hydrogels were prepared by using different contents of the cross-linking agent. Typically, 10.0 g AM, 1.0 g SA, 0.10 g APS, and 50 mL ultrapure water were added to a glass bottle. Then, NMBA with different weights of 0.01, 0.03, 0.05, and 0.30 g were added into the above solutions and stirred until completely dissolved. The hydrogel was then obtained by heating at 50 °C for 2 h. The mechanical properties of the PAM/SA hydrogels with different AM-to-SA ratios and cross-linking agent concentrations were characterized by tensile tests on a universal material testing machine (HY-0659, HENGYI, China), where their stress–strain curves were plotted (Figure S16, Supporting Information).

Preparation of the SC E-Skins: The SC-E-skins were prepared by using different contents of LMPs. In a typical experiment, 10.0 g AM, 1.0 g SA, 0.10 g APS, 0.01 g NMBA, and 25.0 mL ultrapure water were added to a

glass bottle and stirred, obtaining an AM-SA solution. Then, suspensions with different LMPs content (4.0, 8.0, 15.0, 18.0, or 21.0 wt.%) were added into the AM-SA solution and mechanically stirred. Finally, the mixed liquid was put into the structural color layer with a 200-µm spacer and polymerized at room temperature, resulting in the SC E-skins after heating at 50 °C for 30 min for rapid curing of the hydrogel.

Breath Monitoring: The SC E-skins were pasted onto different surfaces (balloons, fingers, and rat's skin). First, the SC E-skins (length × width × thickness = 2 cm × 2 cm × 200 µm) were attached to a balloon. Upon air-blowing the balloon, the relative resistance changes of the SC E-skins were characterized by an LCR digital bridge (TH2830, Tonghui, China) with a voltage of 1 V and a sweep frequency of 10 kHz, and their structural color changes were characterized by a fiber-optic spectrometer (HR 2000+, Ocean Optics, US). Second, the SC E-skins (length × width × thickness = 1.5 cm × 3.5 cm × 200 µm) were pasted on the fingers. The relative resistance changes and the structural color changes of the SC E-skins were detected when the fingers bent. Finally, the SC E-skins (length × width × thickness = 1.3 cm × 1.0 cm × 200 µm) were pasted on the rat's skin. The relative resistance changes and the structural color changes of the SC E-skins along with the breath of the rat were recorded through the similar methods mentioned above. All the experiments involving animals were performed under the approval of the Animal Use and Care Committee of the Shenzhen Institute of Advanced Technology, Chinese Academy of Sciences with the project license (SIAT-IACUC-210301-TGS-ZQL-A1667-01) following ethical review.

Characterization: The macroscopic photos of samples were taken by a digital camera (Canon, EOS 6D, Japan). The microstructures of the samples were characterized by a field emission scanning electron microscope (FE-SEM, Sigma 300, Zeiss, Germany). The distributions of Ga and In elements in the SC E-skins were analyzed by an energy dispersive spectrometer (XFlash, Bruker, Germany). Reflection spectra were measured by an optical microscope (NI-U, Nikon, Japan), equipped with a fiber-optic spectrometer (HR 2000+, Ocean Optics, US). The stress–strain curves and tensile strength of the hydrogel on different substrates such as rubber gloves and porcine skins were obtained by performing tensile tests on the universal material testing machine. The resistance of the samples was measured by an LCR digital bridge (TH2830, Tonghui, China). The sulfate-free radicals were characterized by an EPR spectrometer (Bruker EMX premium X; Germany) with the assistance of DMPO. The coordination bonds of the SC E-skins were characterized by an FTIR spectrometer (Nicolet iS50, Thermo Scientific, US).

Supporting Information

Supporting Information is available from the Wiley Online Library or from the author.

Acknowledgements

The authors acknowledge the financial support provided by National Natural Science Foundation of China (52022102, 52261160380, 52303289), the National Key R&D Program of China (2017YFA0701303), the Youth Innovation Promotion Association of CAS (Y2023100), the Guangdong Regional Joint Fund-Key Project (2021B1515120076), Guangdong Regional Joint Fund-Youth Project (2021A1515110275), the Fundamental Research Program of Shenzhen (RCJC20221008092729033, JCYJ20220818101800001), and the Shenzhen Medical Research Fund (B2302045).

Conflict of Interest

The authors declare no conflict of interest.

Author Contributions

X. D. and Z. L. conceived and supervised the research. Y. S. conducted the experiments with the assistance of C. H. C. H. and Y. S. analyzed the results, and wrote the manuscript. X. D. and Z. L. revised the manuscript. All authors contributed to the discussion and interpretation of the results. Y. S. and C. H. contributed equally to this work.

Data Availability Statement

The data that support the findings of this study are available in the supplementary material of this article.

Keywords

conductive hydrogel, electric–optical sensor, electronic skin, liquid metal, structural color

Received: July 17, 2024
Revised: October 13, 2024
Published online:

[1] F. C. Carlton, *Amer. Acad. Arts & Sci.* **1903**, *39*, 259.
[2] J. Teyssier, S. V. Saenko, D. Marel, M. C. Milinkovitch, *Nat. Commun.* **2015**, *6*, 6368.
[3] M. J. Whiting, B. S. Holland, J. S. Keogh, D. W. A. Noble, *Sci. Adv.* **2022**, *8*, eabn2415.
[4] T. L. Williams, S. L. Senft, J. Yeo, F. J. Martín-Martínez, A. M. Kuzirian, C. A. Martin, C. W. DiBona, C. T. Chen, S. R. Dinneen, H. T. Nguyen, C. M. Gomes, J. J. C. Rosenthal, M. D. MacManes, F. Chu, M. J. Buehler, R. T. Hanlon, L. F. Deravi, *Nat. Commun.* **2019**, *10*, 1004.
[5] M. Fan, D. Stuart-Fox, V. Cadena, *PLoS One* **2014**, *9*, e111504.
[6] B. Shih, D. Shah, J. Li, T. G. Thuruthel, Y. L. Park, F. Lida, Z. Bao, R. K. Bottiglio, M. T. Tolley, *Sci. Robot.* **2020**, *5*, eaaz9239.
[7] Q. Shi, Z. Zhang, Y. Yang, X. Shan, B. Salam, C. Lee, *ACS Nano* **2021**, *15*, 18312.
[8] Y. Jiang, S. Ji, J. Huang, Y. Li, G. Zou, T. Salim, C. Wang, W. Li, H. Jin, J. Xu, S. Wang, T. Lei, X. Yan, W. Y. X. Peh, S. C. Yen, Z. Liu, M. Yu, H. Zhao, Z. Lu, G. Li, H. Gao, Z. Liu, Z. Bao, X. Chen, *Nature* **2023**, *614*, 456.
[9] J. Li, Y. Liu, L. Yuan, B. Zhang, E. S. Bishop, K. Wang, J. Tang, Y. Zheng, W. Xu, S. Niu, L. Beker, T. L. Li, G. Chen, M. Diyaolu, A. L. Thomas, V. Mottini, J. B. H. Tok, J. C. Y. Dunn, B. Cui, S. P. Pasca, Y. Cui, A. Habtezion, X. Chen, Z. Bao, *Nature* **2022**, *606*, 94.
[10] W. Zhou, Y. Jiang, Q. Xu, L. Chen, H. Qiao, Y. Wang, J. Lai, D. Zhong, Y. Zhang, W. Li, Y. Du, X. Wang, J. Lei, G. Dong, X. Guan, S. Ma, P. Kang, L. Yuan, M. Zhang, J. B. H. Tok, D. Li, Z. Bao, W. Jia, *Nat. Biomed. Eng.* **2023**, *7*, 1270.
[11] Z. Zhang, L. Tang, C. Chen, H. Yu, H. Bai, L. Wang, M. Qin, Y. Feng, W. Feng, *J. Mater. Chem. A.* **2021**, *9*, 875.
[12] S. Gong, W. Schwalb, Y. Wang, Y. Chen, Y. Tang, J. Si, B. Shirinzadeh, W. Cheng, *Nat. Commun.* **2014**, *5*, 3132.
[13] Y. Wang, C. Zhu, R. Pfattener, H. Yan, L. Jin, S. Chen, F. M. Lopez, F. Lissel, J. Liu, N. I. Rabiah, Z. Chen, J. W. Chun, C. Linder, M. F. Toney, B. Murmann, Z. Bao, *Sci. Adv.* **2017**, *3*, e1602076.
[14] Y. Zhao, W. Gao, K. Dai, S. Wang, Z. Yuan, J. Li, W. Zhai, G. Zheng, C. Pan, C. Liu, C. Shen, *Adv. Mater.* **2021**, *33*, 2102332.
[15] H. H. Chou, A. Nguyen, A. Chortos, J. W. F. To, C. Lu, J. Mei, T. Kurosawa, W. G. Bae, J. B. H. Tok, Z. Bao, *Nat. Commun.* **2015**, *6*, 8011.
[16] H. Yuk, B. Lu, X. Zhao, *Chem. Soc. Rev.* **2019**, *48*, 1642.
[17] S. Wang, J. Xu, W. Wang, G. J. N. Wang, R. Rastak, F. M. Lopez, J. W. Chung, S. Niu, V. R. Feig, J. Lopez, T. Lei, S. K. Kwon, Y. Kim, A. M. Foudeh, A. Ehrlic, A. Gasperini, Y. Yun, B. Murmann, J. B. H. Tok, Z. Bao, *Nature* **2018**, *555*, 83.

[18] Y. S. Zhang, A. Khademhosseini, *Science* **2017**, *356*, eaaf3627.
[19] D. Wirthl, R. Pichler, M. Drack, G. Kettlguber, R. Moser, R. Gerstmayr, F. Hartmann, E. Bradt, R. Kaltseis, C. M. Siket, S. E. Schausberger, S. Hild, S. Bauer, M. Kaltenbrunner, *Sci. Adv.* **2017**, *3*, e1700053.
[20] J. Shi, Y. Lin, P. Li, P. Mickel, C. Sun, K. Parekh, J. Ma, S. Kim, B. Ashwood, L. Meng, Y. Luo, S. Chen, H. M. Tsai, C. M. Cham, J. Zhang, Z. Cheng, J. A. A. Halimah, J. Chen, P. Griffin, E. B. Chang, P. Král , J. Yue, B. Tian, *Nat. Chem. Eng.* **2024**, *1*, 73.
[21] H. Yuk, J. Wu, X. Zhao, *Nat. Rev. Mater.* **2022**, *7*, 935.
[22] C. Lim, Y. J. Hong, J. Jung, Y. Shin, S. H. Sunwoo, S. Baik, O. K. Park, S. H. Choi, T. Hyeon, J. H. Kim, S. Lee, D. H. Kim, *Sci. Adv.* **2021**, *7*, eabd3716.
[23] G. Gao, F. Yang, F. Zhou, J. He, W. Lu, W. Lu, P. Xiao, H. Yan, C. Pan, T. Chen, Z. L. Wang, *Adv. Mater.* **2020**, *32*, 2004290.
[24] B. Lu, H. Yuk, S. Lin, N. Jian, K. Qu, J. Xu, X. Zhao, *Nat. Commun.* **2019**, *10*, 1043.
[25] C. Yang, Z. Suo, *Nat. Rev. Mater.* **2018**, *3*, 125.
[26] X. Du, H. Cui, Q. Zhao, J. Wang, H. Chen, Y. Wang, *Research* **2019**, *2019*, 6398296.
[27] H. Hu, C. Huang, M. Galluzzi, Q. Ye, R. Xiao, X. Yu, X. Du, *Research* **2021**, *2021*, 9786128.
[28] Y. Zhuang, R. J. Xie, *Adv. Mater.* **2021**, *33*, 2005925.
[29] K. Meng, X. Xiao, W. Wei, G. Chen, A. Nashalian, S. Shen, X. Xiao, J. Chen, *Adv. Mater.* **2022**, *34*, 2109357.
[30] F. Han, T. Wang, G. Liu, H. Liu, X. Xie, Z. Wei, J. Li, C. Jiang, Y. He, F. Xu, *Adv. Mater.* **2022**, *34*, 2109055.
[31] G. Lin, M. Si, L. Wang, S. Wei, W. Lu, H. Liu, Y. Zhang, D. Li, T. Chen, *Adv. Opt. Mater.* **2022**, *10*, 2102306.
[32] G. Su, N. Wang, Y. Liu, R. Zhang, Z. Li, Y. Deng, B. Tang, *Adv. Mater.* **2024**, *36*, 2400085.
[33] Z. Liu, H. Bisoyi, Y. Huang, M. Wang, H. Yang, Q. Li, *Angew. Chem., Int. Ed.* **2022**, *61*, e202115755.
[34] Y. Wang, W. Niu, C. Lo, Y. Zhao, X. He, G. Zhang, S. Wu, B. Ju, S. Zhang, *Adv. Funct. Mater.* **2020**, *30*, 2000356.
[35] H. Zhang, H. Chen, J. H. Lee, E. Kim, K. Y. Chan, H. Venkatesan, X. Shen, J. Yang, J. K. Kim, *ACS Nano* **2023**, *17*, 5921.
[36] Z. Li, Q. Fan, Y. Yin, *Chem. Rev.* **2021**, *122*, 4976.
[37] J. Ge, Y. Yin, *Angew. Chem., Int. Ed.* **2011**, *50*, 1492.
[38] C. Huang, Y. Shang, J. Hua, Y. Yin, X. Du, *ACS Nano* **2023**, *17*, 10269.
[39] Y. Zhao, Z. Xie, H. Gu, C. Zhu, Z. Gu, *Chem. Soc. Rev.* **2012**, *41*, 3297.
[40] Y. Wang, L. Shang, G. Chen, L. Sun, X. Zhang, Y. Zhao, *Sci. Adv.* **2020**, *6*, eaax8258.
[41] K. Chen, Q. Fu, S. Ye, J. Ge, *Adv. Funct. Mater.* **2017**, *27*, 1702825.
[42] Y. Zhang, Q. Fu, J. Ge, *Nat. Commu.* **2015**, *6*, 7510.
[43] M. Su, Y. Song, *Chem. Rev.* **2022**, *122*, 5144.
[44] X. Lai, J. Peng, Q. Cheng, A. P. Tomsia, G. Zhao, L. Liu, G. Zou, Y. Song, L. Jiang, M. Li, *Angew. Chem., Int. Ed.* **2021**, *60*, 14307.
[45] Y. Wang, Q. Zhao, X. Du, *Mater. Horiz.* **2020**, *7*, 1341.
[46] X. Du, H. Cui, T. Xu, C. Huang, Y. Wang, Q. Zhao, Y. Xu, X. Wu, *Adv. Funct. Mater.* **2020**, *30*, 1909202.
[47] M. Nie, C. Huang, X. Du, *Nanoscale* **2021**, *13*, 2780.
[48] Y. Wang, Q. Zhao, X. Du, *J. Mater. Chem. B.* **2020**, *8*, 3519.
[49] Y. Wang, H. Cui, Q. Zhao, X. Du, *Matter* **2019**, *1*, 626.
[50] H. Yi, S.-H. Lee, H. Ko, D. Lee, W.-G. Bae, T.-i. Kim, D. S. Hwang, H. E. Jeong, *Adv. Funct. Mater.* **2019**, *29*, 1902720.
[51] Y. Sun, Y. Wang, Y. Liu, S. Wu, S. Zhang, W. Niu, *Adv. Funct. Mater.* **2022**, *32*, 2204467.
[52] Z. Zhang, Z. Chen, Y. Wang, Y. Zhao, *Proc. Natl. Acad. Sci. USA* **2020**, *117*, 18310.
[53] Y. Wang, Y. Yu, J. Guo, Z. Zhang, X. Zhang, Y. Zhao, *Adv. Funct. Mater.* **2020**, *30*, 2000151.
[54] Y. Dong, A. Bazrafshan, A. Pokutta, F. Sulejmani, W. Sun, J. D. Combs, K. C. Clarke, K. Salaita, *ACS Nano* **2019**, *13*, 9918.
[55] L. Peng, L. Hou, P. Wu, *Adv. Mater.* **2023**, *35*, 2211342.
[56] A. Chortos, J. Liu, Z. Bao, *Nat. Mater.* **2016**, *15*, 937.
[57] H. Zhang, J. Guo, Y. Wang, L. Sun, Y. Zhao, *Adv. Sci.* **2021**, *8*, 2102156.
[58] Y. Hu, H. Zhuo, Y. Zhang, H. Lai, J. Yi, Z. Chen, X. Peng, X. Wang, C. Liu, R. Sun, L. Zhong, *Adv. Funct. Mater.* **2021**, *31*, 2106761.
[59] Y. Y. Choi, D. H. Ho, J. H. Cho, *ACS Appl. Mater. Interfaces* **2020**, *12*, 9824.
[60] J. Ma, Y. Lin, Y.-W. Kim, Y. Ko, J. Kim, K. H. Oh, J. Y. Sun, C. B. Gorman, M. A. Voinov, A. I. Smirnov, J. Genzer, M. D. Dickey, *ACS Macro Lett.* **2019**, *8*, 1522.
[61] X. Du, T. Li, L. Li, Z. Zhang, T. Wu, *J. Mater. Chem. C.* **2015**, *3*, 3542.
[62] X. Li, M. Li, L. Zong, X. Wu, J. You, P. Du, C. Li, *Adv. Funct. Mater.* **2018**, *28*, 1804197.
[63] F. Centurion, R. N. Zangeneh, N. Flores, M. Tajik, S. Merhebi, R. Abbasi, M. Mayyas, F. M. Allioux, J. Tang, W. A. Donald, C. Boyer, M. D. Dickey, K. K. Zadeh, M. A. Rahim, *ACS Appl. Nano Mater* **2021**, *4*, 2987.
[64] M. Wang, Z. Lai, X. Jin, T. Sun, H. Liu, H. Qi, *Adv. Funct. Mater.* **2021**, *31*, 2101957.
[65] P. Rahmani, A. Shojaei, T. Sakorikar, M. Wang, Y. M. Apodaca, M. D. Dickey, *ACS Nano* **2024**, *18*, 8038.
[66] A. Chortos, Z. Bao, *Mater. Horiz.* **2014**, *17*, 321.
[67] H. Wang, Y. Yao, Z. He, W. Rao, L. Hu, S. Chen, J. Lin, J. Gao, P. Zhang, X. Sun, X. Wang, Y. Cui, Q. Wang, S. Dong, G. Chen, J. Liu, *Adv. Mater.* **2019**, *31*, 1901337.
[68] L. Han, M. Wang, L. O. Prieto-López, X. Deng, J. Cui, *Adv. Funct. Mater.* **2020**, *30*, 1907064.
[69] W. Tang, T. Yan, J. Ping, J. Wu, Y. Ying, *Adv. Mater. Tech.* **2017**, *2*, 1700021.
[70] M. Ali, A. Elsayed, A. Mendez, Y. Savaria, M. Sawan, *IEEE Sens. J.* **2021**, *21*, 14569.
[71] L. Hu, P. L. Chee, S. Sugiarto, Y. Yu, C. Shi, R. Yan, Z. Yao, X. Shi, J. Zhi, D. Kai, H. Yu, W. Huang, *Adv. Mater.* **2023**, *35*, 2205326.
[72] W. Ge, S. Cao, Y. Yang, O. J. Rojas, X. Wang, *Chem. Eng. J.* **2021**, *408*, 127306.
[73] X. Sui, H. Guo, C. Cai, Q. Li, C. Wen, X. Zhang, X. Wang, J. Yang, L. Zhang, *Chem. Eng. J.* **2021**, *419*, 129478.
[74] T. Zhu, C. Jiang, M. Wang, C. Zhu, N. Zhao, J. Xu, *Adv. Funct. Mater.* **2021**, *31*, 2102433.
[75] Z. Gu, H. Chen, S. Zhang, L. Sun, Z. Xie, Y. Ge, *Colloid Surface A.* **2007**, *302*, 312.
[76] X. Li, M. Li, J. Xu, J. You, Z. Yang, C. Li, *Nat. Commun.* **2019**, *10*, 3514.
[77] F. Wang, M. Liu, C. Liu, Q. Zhao, T. Wang, Z. Wang, X. Du, *Sci. Adv.* **2022**, *8*, eabp9369.
[78] F. Wang, M. Liu, C. Liu, C. Huang, L. Zhang, A. Cui, Z. Hu, X. Du, *Natl. Sci. Rev.* **2023**, *10*, nwac164.
[79] H. Hu, M. Nie, M. Galluzzi, X. Yu, X. Du, *Adv. Funct. Mater.* **2023**, *33*, 2304634.